Inorganic Chemistry

Article

pubs.acs.org/IC

Mechanisms of the Water-Gas Shift Reaction Catalyzed by Ruthenium Pentacarbonyl: A Density Functional Theory Study

Hannes Schulz, Andreas Görling, and Wolfgang Hieringer*

Lehrstuhl für Theoretische Chemie, Department Chemie und Pharmazie, Universität Erlangen-Nürnberg, Egerlandstraße 3, 91058 Erlangen, Germany

Supporting Information

ABSTRACT: The mechanism of the water-gas shift reaction catalyzed by $Ru(CO)_5$ is analyzed using density functional methods in solution within the conductor-like screening model. Four different mechanistic pathways have been considered. It turned out that the incorporation of solvent effects is very important for a reasonable comparison among the mechanistic alternatives. The explicit inclusion of a water solvent molecule significantly changes the barriers of those steps which involve proton transfer in the transition state. The corresponding barriers are either lowered or increased, depending on the structure of the corresponding cyclic transition states. The results show that protolysis steps become competitive due to solution effects. The formation of formic acid as an intermediate in another, alternative pathway is also found to be competitive.

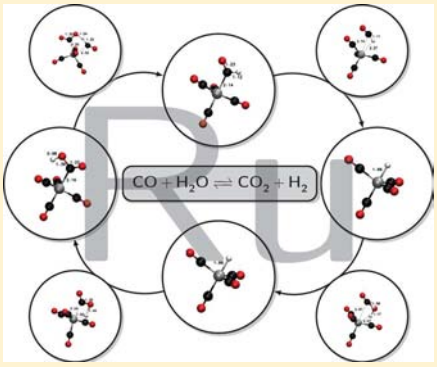

1. INTRODUCTION

The water-gas shift reaction (WGSR) (Scheme 1) is an important industrial process for the production of hydrogen gas

Scheme 1. Water-Gas Shift Reaction

$$CO + H_2O \longrightarrow CO_2 + H_2 \quad \Delta H_R = -41\ kJmol^{-1}$$

from water and carbon monoxide and for the removal of carbon monoxide from technical gas mixtures such as water gas, which is a primary source of the world's hydrogen supply.[1] The availability of hydrogen feedstocks with low CO contaminant levels is also relevant in important technical processes such as ammonia synthesis. An upcoming application of the WGSR is its use for H_2 production for mobile applications employing fuel cells. Here, the hydrogen produced in the in situ steam reforming of classical car fuels contains up to 20% CO, which poisons the fuel cells, and the water-gas shift reaction is used to decrease the CO content.

The WGSR is an exothermic reaction ($\Delta H_R = -41$ kJ/mol), and hence H_2 production and CO consumption is most effective at low temperatures. Therefore, the availability of catalysts which facilitate the reaction at low temperatures is a key question in water-gas shift chemistry. On the industrial scale, the reaction is usually facilitated by heterogeneous catalysts.[1c,d] The discovery that metal carbonyls such as $Fe(CO)_5$ and $Ru(CO)_5$ bear the potential to catalyze the reaction at low temperatures has triggered increasing interest in the homogeneously catalyzed WGSR, which led to a number of mechanistic studies.[1a,b,2] The homogeneous WGSR can be conducted in acidic or basic media, the latter usually being more efficient.

Theoretical studies have contributed much to a better understanding of the homogeneous WGSR catalyzed by $Fe(CO)_5$. This field has been pioneered by three studies on the gas-phase mechanisms of the base-induced WGSR catalyzed by $Fe(CO)_5$. A groundbreaking theoretical study by Torrent at al.[3] closely followed the classical mechanistic proposal which had been investigated experimentally by Sunderlin and Squires.[2b] This mechanism involves a hydroxide dissociation step which had been found highly unfavorable in the gas phase.[2b,3] Subsequently, two other theoretical studies proposed alternative reaction pathways which avoid the dissociation of hydroxide. Barrows proposed a two-step mechanism[4] which furthermore provides an explanation for the first-order rate dependence on CO pressure as observed in some experiments. In a recent study, Rozanska et al. have carefully reanalyzed previous mechanistic proposals, including formic acid formation.[5] In the same study, the authors have also proposed yet another mechanism which was reported to be even more favorable (in the gas phase at least) than those that had been investigated theoretically before. Very recently, one of the reaction pathways suggested in ref 5a has been studied for metal carbonyls $M(CO)_5$ with M = Fe, Ru, Os, finding that $Os(CO)_5$ is not a suitable catalyst for the WGSR along that pathway.[6] Moreover, the effect of metal−metal cooperativity has been investigated theoretically in the iron carbonyl catalyzed WGSR.[7]

Experimental evidence shows that ruthenium carbonyls—the simplest example being $Ru(CO)_5$—might be more effective catalysts than $Fe(CO)_5$ for the homogeneous WGSR.[1c]

Received: July 15, 2012
Published: April 19, 2013

dx.doi.org/10.1021/ic301539q | Inorg. Chem. 2013, 52, 4786−4794

Scheme 2. Classical Mechanism A Following Torrent et al.[3a]

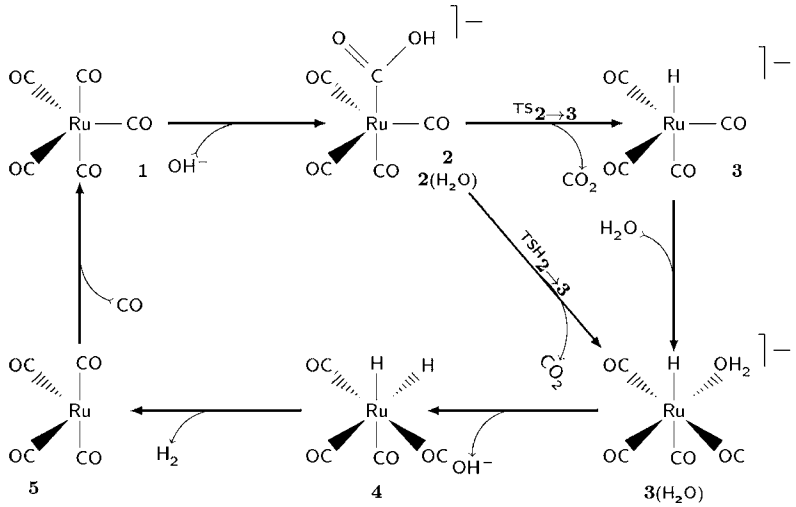

[a]Intermediates are labeled by numbers *x*. The intermediate labeled **2**(H_2O) represents an alternative to intermediate **2** containing an additional water molecule which is not explicitly shown in the formula. See Figures 1 and 2 for the optimized structures of all intermediates and transition states.

Recently, the interest in these ruthenium catalysts underwent a revival due to the discovery of ruthenium-based ultra-low-temperature WGSR catalysts in ionic liquid solution rather than the usual organic solvents by Werner et al.[8] The mechanism of ruthenium carbonyl catalyzed WGSR is less well understood, however. The nature of the active species is less clear than in the Fe case, due to the tendency of Ru to favor polynuclear carbonyl clusters such as $Ru_3(CO)_{12}$ and $Ru_2(CO)_8$, which are in equilibrium with $Ru(CO)_5$.[9] In order to allow for a further optimization of such catalytic systems, an understanding of the underlying reaction mechanism appears necessary.

In this work, we investigate the base-induced ruthenium carbonyl catalyzed water-gas shift reaction using an approximate solvation model. Experimentally, the reaction is usually carried out in wet organic solvents or, very recently, in ionic liquid solutions.[8] We analyze four mechanistic proposals which correspond to those investigated theoretically earlier for the $Fe(CO)_5$ case. As mentioned, ruthenium carbonyls are well-known to favor multinuclear carbonyl clusters,[9,10] and an equilibrium can be assumed among mononuclear $Ru(CO)_5$ and di- or trinuclear species, leading to a great complexity of possible active species and pathways. In this study on the Ru carbonyl catalyzed WGSR, we reduce this complexity by simply assuming $Ru(CO)_5$ as the catalyst precursor and completely ignore the possible role of ruthenium carbonyl clusters. The experimental equilibrium constant for trimerization has been determined to be 3×10^6 mol/L in *n*-heptane at 298 K and at standard pressure.[10] Of course, under CO pressure (as in typical WGSR conditions) the equilibrium will be shifted in favor of $Ru(CO)_5$. Moreover, the catalytically active species need not necessarily be the thermodynamically most stable species. Indeed, experimental evidence has led to speculations about the possibility of $Ru(CO)_5$ as the active species.[1a] It has also been argued that $Ru_3(CO)_{12}$ is possibly not the active species for WGSR, and several simpler metal carbonyls have been favored.[1b,11]

This paper is organized as follows. We first provide information on the theoretical approach chosen here to model the $Ru(CO)_5$-catalyzed WGSR in solution. We then discuss in detail the mechanistic pathways investigated and report our results on reaction energies and activation barriers for each individual step. We analyze the results in terms of the predicted turnover frequency for each of the alternative mechanistic pathways and compare our findings to $Fe(CO)_5$ catalysis. We close our report with a conclusion.

2. COMPUTATIONAL DETAILS

All calculations in this study have been performed using density functional theory as implemented in the TURBOMOLE program package.[12] The approximate exchange and correlation functionals of Becke[13] and Perdew,[14] denoted BP86 in this work, has been employed as a standard functional throughout this work unless stated otherwise. Additional data from calculations using the B3LYP[15] hybrid functional are shown as stated in the text. Full results obtained with the B3LYP functional can be found in the Supporting Information. A basis set of augmented triple-ζ quality (aug-TZVPP) has been used throughout, which is composed of the def2-TZVPP[16] basis set from the TURBOMOLE library and diffuse functions taken from the aug-cc-pVTZ[17] basis set for H, C, and O, while the central Ru atom was left unaugmented. Calculations using the BP86 functional have been performed with the resolution of the identity (RI) approximation. Solvation effects have approximately been taken into account by the COSMO approach,[18] using a solvent permittivity of 12, which is an estimate for an ionic liquid solvent.[19] This choice has been made in the light of recent reports of Ru-based low-temperature WGSR catalysis in supported ionic liquids.[8] While the inclusion of solvent effects turned out to be crucial, as will be discussed later on, the precise choice of solvent permittivity in COSMO was found to be of limited importance for most reactions studied here. A comparison of results obtained with the dielectric constant of water, ionic liquid, and the gas phase can be found in the Supporting Information. All minimum geometries and transition states have been fully optimized without any constraints, and the nature of each stationary point has been verified by subsequent frequency calculations using the aoforce or NumForce programs of TURBOMOLE. All energy differences quoted (ΔE, $\Delta E^{\ddagger}$) include the corresponding zero-point vibrational energy (corresponding to enthalpies at 0 K). Free energies (ΔG, $\Delta G^{\ddagger}$) have been calculated from the standard gas-phase (ideal gas) formulas for room temperature (298.15 K) and ambient pressure (0.1 MPa) using the freeh module; the calculated vibrational frequencies have not been scaled. Further information on the effects of different basis sets and the density functional used, the importance of solvation effects, and the effects of free energy corrections can be found in the Supporting Information.

dx.doi.org/10.1021/ic301539q | *Inorg. Chem.* 2013, 52, 4786−4794

Scheme 3. Mechanistic Proposal B Following Barrows[4a]

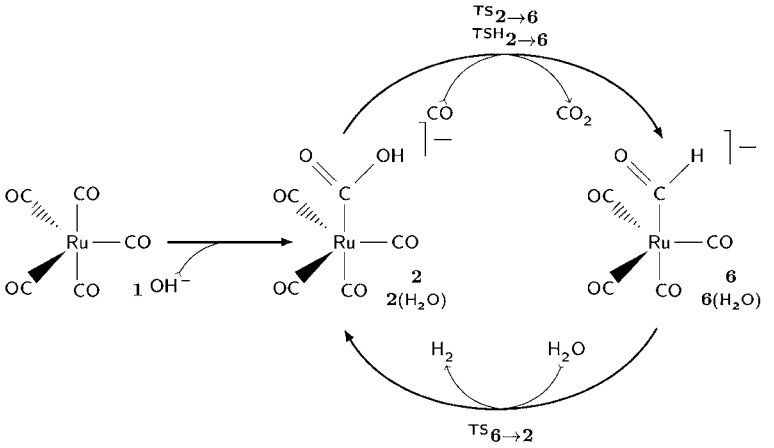

[a]Intermediates are labeled by numbers ***x***. The intermediates labeled ***x***(H_2O) represent an alternative to intermediate ***x*** containing an additional water molecule which is not explicitly shown in the formulas. See Figures 1 and 2 for the optimized structures of all intermediates and transition states.

Scheme 4. Mechanistic Proposal C Following Rozanska et al.[5a a]

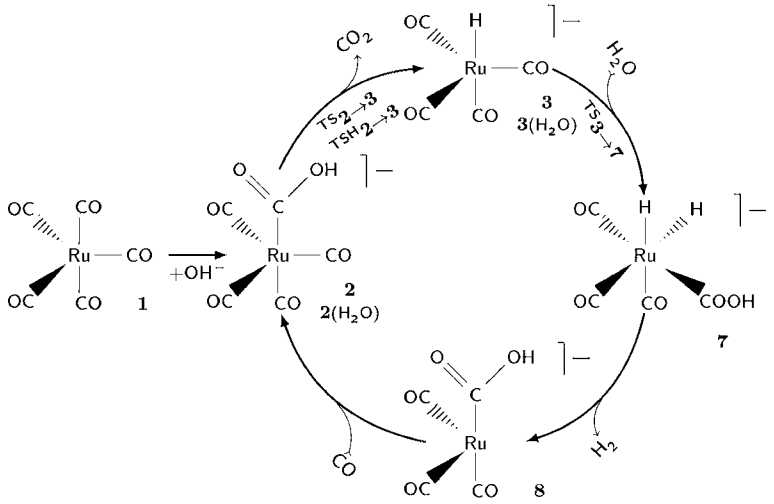

[a]Intermediates are labeled by numbers ***x***. The intermediates labeled ***x***(H_2O) represent an alternative to intermediate ***x*** containing an additional water molecule which is not explicitly shown in the formulas. See Figures 1 and 2 for the optimized structures of all intermediates and transition states.

3. RESULTS

The four distinct mechanistic pathways for the $Ru(CO)_5$-catalyzed WGSR investigated in this study, labeled A–D, are shown in Schemes 2–5. They closely follow the mechanistic proposals brought forward in earlier studies on $Fe(CO)_5$ catalysis.[3−5] We first summarize the key features of each of these mechanistic proposals and subsequently present the computed reaction energies and activation barriers for each step. The optimized structures of key intermediates and transition states are shown in Figures 1 and 2, along with some selected bond lengths. The full set of optimized Cartesian coordinates can be found in the Supporting Information.

All mechanistic proposals involve an initial attack of hydroxide OH^- on $Ru(CO)_5$, yielding the metallocarboxylic acid **2**. From here, different pathways are considered. Both the classical mechanism A (Scheme 2) as well as the mechanisms C and D proposed by Rozanska (Schemes 4 and 5) proceed through a decarboxylation of metallocarboxylic acid **2** to form hydride species **3**. The latter then can react with water in two distinct ways. Following the classical mechanism,[3] protolysis of the base **3** proceeds by first coordinating a water molecule to the Ru center and by subsequent release of hydroxide, leaving dihydride complex **4**, which finally undergoes reductive elimination of H_2 and recoordination of a CO ligand.

For Fe catalysis, the protolysis of **3** with H_2O was shown to be very endothermic in the gas phase[2b,3] due to the release of unsolvated hydroxide. It was clear, however, that the gas-phase thermodynamic data will differ considerably for the corresponding solution thermodynamics. Nevertheless, Rozanska et al.[5a] investigated a new pathway where protolysis does not involve release of hydroxide. Following their suggestion (Scheme 4), H_2O undergoes a dissociative nucleophilic attack on one of the remaining CO ligands in hydride complex **3** to form species **7**. The latter complex subsequently releases H_2 to form the metallocarboxylic acid **8**, and **2** is finally regenerated by recoordination of CO, thereby closing the catalytic cycle.

dx.doi.org/10.1021/ic301539q | Inorg. Chem. 2013, 52, 4786–4794

Scheme 5. Mechanistic Proposal D Involving a Formic Acid Mechanism, Following Rozanska et al.[5aa]

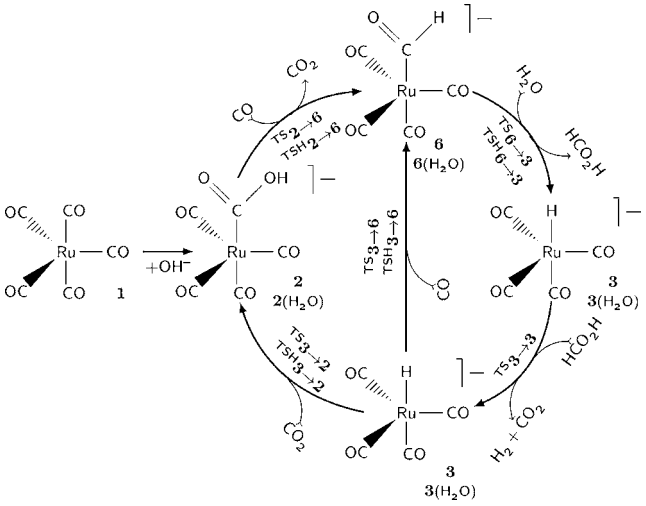

[a]Intermediates are labeled by numbers ***x***. The intermediates labeled ***x***(H_2O) represent an alternative to intermediate ***x*** containing an additional water molecule which is not explicitly shown in the formulas. See Figures 1 and 2 for the optimized structures of all intermediates and transition states.

Mechanism B (Scheme 3) is a two-step mechanism starting from metallocarboxylic acid **2** to yield the formyl species **6** by carbonylation of **2** and concerted decarboxylation. **6** then reacts with a water molecule with simultaneous release of hydrogen to regenerate **2**, thereby completing the catalytic cycle.

Yet another mechanistic alternative, D (Scheme 5), involves a nucleophilic attack of H_2O on the formyl group of **6**, leading to a decomposition of the latter into formic acid and **3**.[11] Formic acid in turn is decomposed into the WGSR products CO_2 and H_2 with the aid of **3**. To close the catalytic cycle, **3** is assumed to form **6** via **2** or, alternatively, by hydrometalation of CO with **3**. In the latter case, **2** is not part of the productive catalytic cycle (see the right side of Scheme 5).

Before we discuss the energy profiles associated with the various reaction cycles of the $Ru(CO)_5$-catalyzed WGSR, we analyze the potential role of water molecules on the activation barriers for the steps in Schemes 2−5, which turns out to be significant.

3.1. Role of Water Molecules in the Transition States. Most of the critical steps to be considered in the WGSR involve a transfer of hydrogen in the transition state. It is well-known that such steps may be affected by the presence or absence of water.[20] We have therefore investigated the relevant transition states in two different variants, labeled $\mathbf{TS}_{x\rightarrow y}$ and $\mathbf{TSH}_{x\rightarrow y}$ (see Figure 2). The difference is that in the second variant ($\mathbf{TSH}_{x\rightarrow y}$) an explicit water molecule is incorporated into the cyclic transition states, thereby expanding the effective ring size in the transition state. In other words, the water molecule becomes part of the transition state and functions as a relay for the hydrogen (proton) transfer within the transition state. Table 1 shows that this leads to significant changes in the resulting activation barriers.

It can be seen from Table 1 that, with one exception, all considered activation energies are lowered by the incorporation of water in the transition states in comparison to the water-free reaction by 21−33 kJ/mol. In contrast, the energy of water-containing $\mathbf{TSH}_{2\rightarrow 6}$ (**2** + CO → **6** + CO_2; Figure 2 and Schemes 2 and 5) is *higher* than that of water-free $\mathbf{TS}_{2\rightarrow 6}$ by 25 kJ/mol: i.e., the incorporation of a water molecule in the transition state slows down the first step in mechanisms B and D (cf. Schemes 3 and 5). Note that the effect of coordinated water on the energies of the reactants is minor in general (up to 3 kJ/mol, data not shown); thus, the effects seen in Table 1 are entirely due to a stabilization or destabilization of the transition states.

These observations may be rationalized on the basis of the ring size that is being formed by the active atoms in the transition state. In those cases where the activation energy is lowered, the incorporation of H_2O into the transition state results in an expansion of the ring from three or four members to a five- or six-membered ring. This may be considered as lowering the ring tension in the transition state, therefore leading to a stabilization. In transition state $\mathbf{TS}_{2\rightarrow 6}$, which is not stabilized by water incorporation, the ring size is expanded from five (−Ru−C−O−H−C−; cf. Figure 2) to seven members, which is obviously less stable. To some extent, this goes in analogy with organic hydrocarbon chemistry, where 5- and 6-rings are known to be more stable than smaller or larger rings. This analogy is only formal, however, because the atoms in the transition states considered here are not carbon and hence may have different optimal binding geometries and steric demands.

Note that the participation of protic reagents (such as H_2O) has been discussed in the iron carbonyl catalyzed WGSR,[3] and experimental data on gas-phase ion chemistry appear to provide evidence *against* the prevalence of such a proton relay mechanism in the decarboxylation reaction of the Fe analogue of **2**.[21] Other experimental evidence suggests decarboxylation takes place via deprotonated (i.e., dianionic) $\mathbf{2}^-$, again without H_2O assistance.[22] This seemingly is in contrast with our results, which do show a lowering in the activation energy. On the other hand, the incorporation of a water molecule (from the solvation shell or coordination sphere) into the transition state may also go along with an entropic penalty and thus may affect the relevant free energies of activation. These effects are difficult to quantify using our present methodology, however, and we therefore leave such entropic effects aside in this study.[23]

In light of our computational results and since water is ubiquitous in WGSR environments, in the following we discuss only those transition state alternatives which lead to the lowest barriers (with or without water) and hence to faster reaction rates. Furthermore, we label all species ***x*** (**1**−**8**) which bear an additional (loosely coordinated) water molecule with a subscript H, $\boldsymbol{x}_{\mathbf{H}}$ (cf. Figures 1 and 2).

3.2. Reaction Energies and Activation Barriers. Figure 3 shows the computed energy profiles associated with the considered catalytic cycles outlined in Schemes 2−5. Reaction energies and activation barriers are given in Table 2. The initial nucleophilic attack of hydroxide at $Ru(CO)_5$ (**1**) to yield the carboxylic acid **2**, which is common to all mechanistic proposals, is exothermic by ΔE = −95 kJ/mol (ΔG = −17 kJ/mol) when solvent effects are included (see section 2 for details). Note that the exothermicity of this step is much smaller than in the gas phase (cf. the Supporting Information and refs 2b and 3). Torrent et al. have found the nucleophilic addition of OH^- to $Fe(CO)_5$ to be barrierless[3] in the gas phase. In solution, however, a linear transit calculation on the present system clearly reveals a barrier for the reaction **1** + OH^- → **2**. A transition state optimization yields an activation barrier of $\Delta E^{\ddagger}$ = 59 kJ/mol ($\Delta G^{\ddagger}$ = 62 kJ/mol). As we will see, however, this

dx.doi.org/10.1021/ic301539q | Inorg. Chem. 2013, 52, 4786−4794

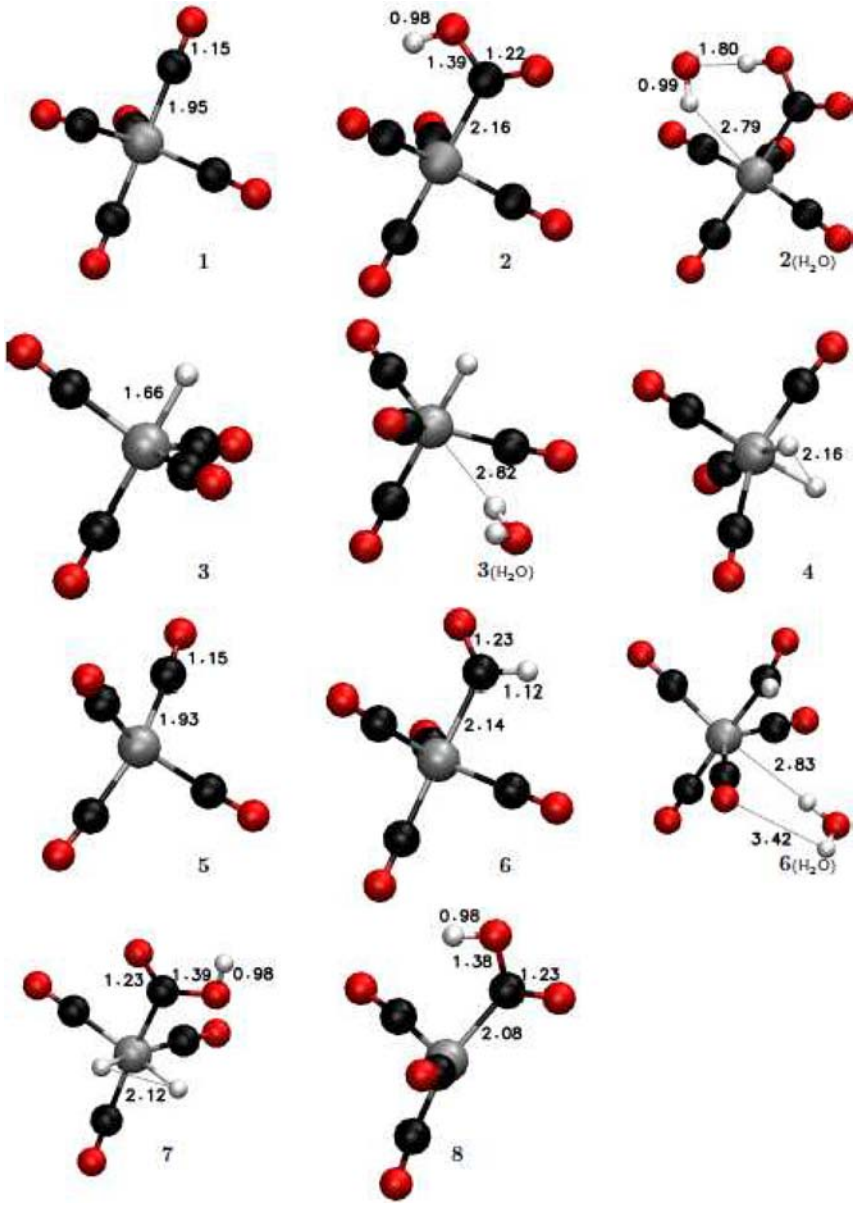

Figure 1. Optimized geometries of WGSR-related intermediates **1**–**8** (cf. Schemes 2–5 for formulas and labeling). Interatomic distances are given in Å. Color code: red, oxygen; black, carbon; gray, ruthenium; white, hydrogen.

barrier is small compared to those of the subsequent steps and hence will not be considered any further.

From metallocarboxylic acid **2**, mechanism B (Scheme 3) proceeds with oxidation of CO by **2** (**2** + CO → **6** + CO_2), which is calculated to be exothermic by $\Delta E = -46$ kJ/mol ($\Delta G = -38$ kJ/mol). This reaction is associated with a fairly low energy barrier of $\Delta E = 75$ kJ/mol ($\Delta G = 119$ kJ/mol). The subsequent step, reduction of H_2O by **6** (**6** + H_2O → **2** + H_2) is again slightly exothermic ($\Delta E = -19$ kJ/mol, $\Delta G = +1$ kJ/mol) but is associated with a substantial barrier of $\Delta E^{\ddagger} = 173$ kJ/mol ($\Delta G^{\ddagger} = 221$ kJ/mol). This reaction completes the two-step WGSR catalytic cycle B. Hence, the latter step must be considered the highest barrier step along this path.

Alternatively, both the classical mechanism A (Scheme 2) and the Rozanska proposals C and D (Schemes 4 and 5) proceed by decarboxylation of carboxylic acid **2** to yield the hydride complex **3** (**2** → **3** + CO_2). This step is calculated to be slightly exothermic ($\Delta E = -32$ kJ/mol, $\Delta G = -65$ kJ/mol) and is associated with a low barrier of only $\Delta E^{\ddagger} = 59$ kJ/mol ($\Delta G^{\ddagger} = 62$ kJ/mol). There has been some debate about the mechanism of the decarboxylation reaction in the Fe analogue of **2**. Evidence for a concerted β-H elimination of CO_2 from the carboxylic acid rather than from the dianion has been given;[24] on the other hand, evidence for decarboxylation proceeding from the dianion was also presented.[21,22] According to our data, however, decarboxylation of **2** is a fairly low-barrier process in the present system anyway, and hence we have not attempted to find any alternative mechanism which might show an even lower activation barrier.

Moving forward along the classical mechanism A (Scheme 2), protolysis of hydride complex **3** proceeds with water coordination ($\Delta E = -3$ kJ/mol) and the dissociation of hydroxide to yield the dihydride complex **4**. The latter step is endothermic ($\Delta E = +114$ kJ/mol; $\Delta G = +86$ kJ/mol) even when including the approximate solvation correction, but much less endothermic than in the gas phase ($\Delta E = +307$ kJ/mol,

dx.doi.org/10.1021/ic301539q | *Inorg. Chem.* 2013, 52, 4786–4794

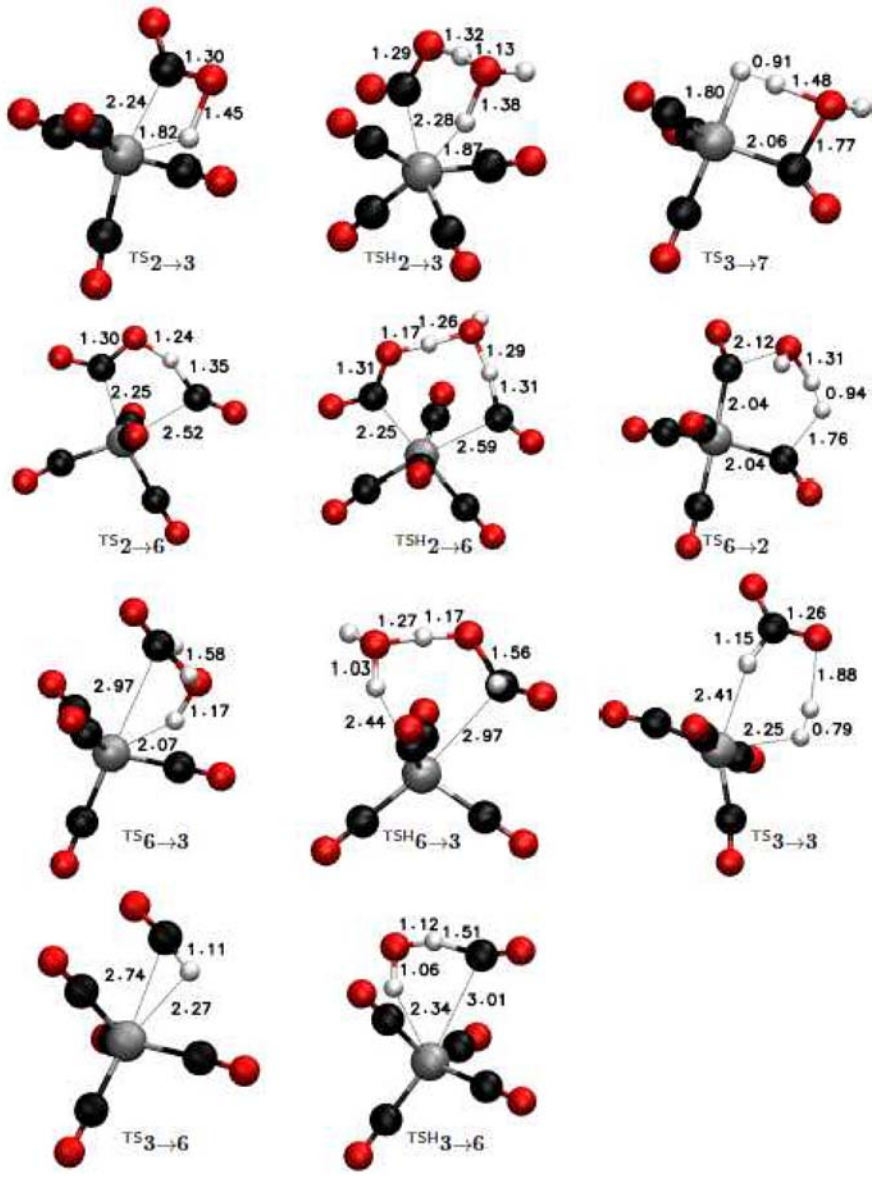

Figure 2. Optimized geometries of WGSR-related transition states (cf. Schemes 2−5 for formulas and labeling). Interatomic distances are given in Å. Color code: red, oxygen; black, carbon; gray, ruthenium; white, hydrogen.

Table 1. Activation Barriers with and without Additional Water in kJ/mol and Corresponding Ring Sizes in the Transition States[a]

			activation energy $\Delta E^{\ddagger}$	
reaction	path(s)	transition states	without H_2O ($\mathbf{TS}_{x\rightarrow y}$)	with H_2O ($\mathbf{TSH}_{x\rightarrow y}$)
2 → **3** + CO_2	A	$\mathbf{TS}_{2\rightarrow 3}$, $\mathbf{TSH}_{2\rightarrow 3}$	92 (4-ring)	**59 (6-ring)**
3 + CO → **6**	D	$\mathbf{TS}_{3\rightarrow 6}$, $\mathbf{TSH}_{3\rightarrow 6}$	170 (3-ring)	**146 (5-ring)**
6 + H_2O → **3** + HCOOH	D	$\mathbf{TS}_{6\rightarrow 3}$, $\mathbf{TSH}_{6\rightarrow 3}$	164 (4-ring)	**143 (6-ring)**
2 + CO → **6** + CO_2	B, D	$\mathbf{TS}_{2\rightarrow 6}$, $\mathbf{TSH}_{2\rightarrow 6}$	**50 (5-ring)**	75 (7-ring)

[a]Cf. Figure 2 for optimized transition structures $\mathbf{TS}_{x\rightarrow y}$ and $\mathbf{TSH}_{x\rightarrow y}$; the lower barrier in each line is given in boldface type.

ΔG = +288 kJ/mol; see the Supporting Information for further gas-phase and solvent effect data and see also previous studies on Fe-catalyzed WGSR[2b,3]). Since we have not been able to locate a transition state for this reaction, we have performed a linear transit calculation in order to obtain an estimate of the activation energy. This procedure[25] provides an (upper) estimate of the activation barrier of 151 kJ/mol. Amovilli et al. have estimated the energy barrier for the Fe case on the basis of approximate reaction path calculations at the CASSCF and HF level and find a barrier of 14 kJ/mol for the *reverse* path ($\mathbf{4}_{Fe}$ + OH^- → $\mathbf{3}_{Fe}$) using a different approximate solution model.[26] This compares with 37 kJ/mol calculated for the present case. In the gas phase, the same reverse process was found to be barrierless, in agreement with our own results.

The next step in the classical mechanism A is hydrogen elimination from dihydride complex **4** to yield $Ru(CO)_4$ (**5**),

dx.doi.org/10.1021/ic301539q | *Inorg. Chem.* 2013, 52, 4786−4794

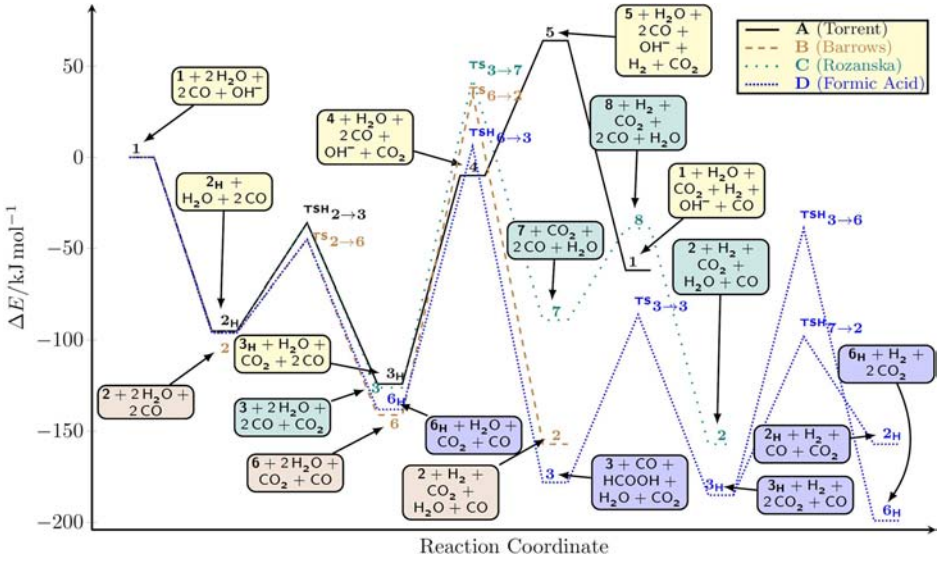

Figure 3. Relative energies of intermediates and transition states according to the mechanistic pathways shown in Schemes 2−5; see the Supporting Information for free energies.

Table 2. Reaction (Free) Energies and Activation (Free) Barriers in kJ/mol for the Steps Shown in Schemes 2−5[a]

path[b]	reaction	ΔE	ΔG	$\Delta E^{\ddagger}$	$\Delta G^{\ddagger}$
A	**1** + OH^- → **2**	−96	−57		
	1 + OH^- + H_2O → $\mathbf{2_H}$	−95	−17		
	$\mathbf{2_H}$ → $\mathbf{3_H}$ + CO_2	−32	−65	59	62
	$\mathbf{3_H}$ → **4** + OH^-	+114	+86	151[c]	
	4 → **5** + H_2	+74	+43		
	5 + CO → **1**	−126	−85		
B	**2** + CO → **6** + CO_2	−50	−36	50	93
	$\mathbf{2_H}$ + CO → $\mathbf{6_H}$ + CO_2	−46	−38	75	115
	6 + H_2O → **2** + H_2	−16	−1	173	221
	$\mathbf{6_H}$ + H_2O → $\mathbf{2_H}$ + H_2	−19	+1		
C	$\mathbf{2_H}$ → **3** + CO_2 + H_2O	−35	−101	59	62
	$\mathbf{2_H}$ → $\mathbf{3_H}$ + CO_2	−32	−65	59	62
	3 + H_2O → **7**	+37	+80	169	212
	$\mathbf{3_H}$ + H_2O → **7** + H_2O	+35	+44	166	176
	7 → **8** + H_2	+50	+20		
	8 + CO + H_2O → $\mathbf{2_H}$	−117	−36		
D	$\mathbf{6_H}$ + H_2O → **3** + HCOOH + H_2O	−40	−79	160	168
	$\mathbf{6_H}$ + H_2O → $\mathbf{3_H}$ + HCOOH	−37	−42	143	194
	3 + HCOOH + H_2O → $\mathbf{3_H}$ + CO_2 + H_2	−11	+15	91	137
	$\mathbf{3_H}$ + HCOOH → $\mathbf{3_H}$ + CO_2 + H_2	−14	−21	89	100
	$\mathbf{3_H}$ + CO → $\mathbf{6_H}$	−14	+26	146	193
	$\mathbf{3_H}$ + CO_2 → $\mathbf{2_H}$	+32	+65	91	127

[a]Cf. also Figure 3 for a reaction energy profile. [b]Label of the mechanistic alternative in which the given reaction (column 2) occurs for the first time in this report. [c]Estimated via linear transit; see main text for details.

which is endothermic by ΔE = +74 kJ/mol (ΔG = +43 kJ/mol). Also here, we have been unable to find the corresponding transition state. Indeed, an approximate linear transit calculation[27] shows no maximum along the Ru···H_2 coordinate, which suggests an essentially barrierless elimination. Energy barriers for H_2 reductive elimination from the analogous Fe complex have been reported below 40 kJ/mol.[3,5a] This is in line with barriers for H_2 reductive elimination in other transition-metal complexes, which are usually found below 50 kJ/mol.[28] We therefore expect that this step is not a high-barrier process in our case. Finally, the mechanism A is completed by exothermic recoordination of CO to $Ru(CO)_4$, which is computed to yield 126 kJ/mol (ΔG = −85 kJ/mol) at the present theoretical level (cf. the Supporting Information for a comparison with experimental data on this reaction).

In total, the step **3** → **4** + OH^- is the highest-barrier step in the classical mechanism A for the present Ru case when including approximate (continuum) solvation effects (cf. section 2). Please note, however, that the endothermicity of this step may further decrease by solvation of hydroxide by explicit water or other solvent molecules. As shown in the Supporting Information, the effect of a single solvating water molecule amounts to an additional 31 kJ/mol stabilization of hydroxide at the present theoretical level.

We now turn to the mechanistic alternative C outlined in Scheme 4. From hydride complex **3**, the next step along this path involves the nucleophilic attack of water on one of the CO ligands in **3**, thereby yielding the dihydrido carboxylic acid **7**. This step is calculated to be endothermic by +35 kJ/mol (ΔG = +44 kJ/mol), and it is associated with the largest barrier along path C ($\Delta E^{\ddagger}$ = 166 kJ/mol; $\Delta G^{\ddagger}$ = 176 kJ/mol). Note that we have found species **7** as a dihydride complex for Ru as the central metal, while it had been found to be a dihydrogen complex for Fe as the central metal.[5a,6] (See ref 29 for discussions of dihydride/dihydrogen complexes of transition metals.) The next step involves hydrogen elimination to yield the coordinatively unsaturated carboxylic acid **8**, which is endothermic by +50 kJ/mol (ΔG = +20 kJ/mol). As before, we have not been able to find a transition state for this reaction, which again suggests a very low activation barrier for this process. The Rozanska-type catalytic cycle C is completed by recoordination of CO to **8** (ΔE = −117 kJ/mol, ΔG = −36 kJ/mol), thereby regenerating the metallocarboxylic acid **2**.

Following experimental evidence,[11] Rozanska et al. in their study on iron complex catalyzed WGSR have also discussed the possibility of *formic acid* formation via yet a different mechanism.[5a] We have investigated this path D (Scheme 5) for the present Ru-catalyzed system. The formic acid path is

dx.doi.org/10.1021/ic301539q | Inorg. Chem. 2013, 52, 4786−4794

assumed to start from carboxylic acid **2** to yield formyl complex **6** by the same reaction as has been discussed before in mechanism B (Scheme 3, barrier $\Delta E^{\ddagger}$ = 75 kJ/mol, $\Delta G^{\ddagger}$ = 119 kJ/mol). **6** is then assumed to react with water to yield the hydride complex **3** and formic acid (**6** + H_2O → **3** + HCOOH), which is an exothermic process (ΔE = −37 kJ/mol, ΔG = −42 kJ/mol). This step is associated with a substantial barrier of $\Delta E^{\ddagger}$ = 143 kJ/mol ($\Delta G^{\ddagger}$ = 194 kJ/mol). **3** in turn catalyzes the decomposition of formic acid into CO_2 and H_2, which is associated with a barrier of $\Delta E^{\ddagger}$ = 89 kJ/mol ($\Delta G^{\ddagger}$ = 100 kJ/mol) and a reaction energy of ΔE = −14 kJ/mol (ΔG = −21 kJ/mol). As already noted by Rozanska et al., this decomposition is favored by low total pressures.[5a] To complete the catalytic cycle, **3** can either undergo hydrometalation of CO to directly regenerate formyl complex **6** or hydrometalation of CO_2 to yield **2**, which can then react further along the lines described before. The former reaction (**3** + CO → **6**) is exothermic (ΔE = −14 kJ/mol) but endoergic (ΔG = 26 kJ/mol) and has a high barrier of $\Delta E^{\ddagger}$ = 146 kJ/mol ($\Delta G^{\ddagger}$ = 193 kJ/mol). The latter reaction, on the other hand, which is the reverse process of the decarboxylation described before, is endothermic by 32 kJ/mol (ΔG = 65 kJ/mol) and has a lower activation barrier of only $\Delta E^{\ddagger}$ = 91 kJ/mol ($\Delta G^{\ddagger}$ = 127 kJ/mol). Both processes are bimolecular association reactions and hence are favored by high total pressures. Note that, in most technical reaction systems, the CO partial pressure will likely be kept high and the CO_2 and H_2 partial pressures will be kept low, such that the reaction **3** + CO → **6** may be favored kinetically over **3** + CO_2 → **2** despite its higher barrier.

For comparison, we have also calculated the energetics of all mechanistic pathways using the B3LYP hybrid functional. The results of these calculations can be found in the Supporting Information. A comparison of the mechanistic pathways just discussed using data from both functionals, as well as a comparison with $Fe(CO)_5$ catalysis, is presented in section 4.

4. DISCUSSION

The previous section has provided a basis for identifying those steps in each mechanistic proposal of Ru-catalyzed WGSR which are associated with the highest activation barriers in the reaction sequence. These steps are the hydroxide dissociation step **3** → **4** + OH^- (or, equivalently, proton transfer **3** + H_2O → **4** + OH^-; see Scheme 2) for the classical mechanism A ($\Delta E^{\ddagger} \approx$ 150 kJ/mol), the reaction of formyl complex **6** with water in mechanism B (**6** + H_2O → **2** + H_2, $\Delta E^{\ddagger}$ = 173 kJ/mol; Scheme 3), the reaction of hydride complex **3** with water in mechanism C (**3** + H_2O → **7**, $\Delta E^{\ddagger}$ = 166 kJ/mol; Scheme 4), or formic acid formation by reaction of formyl complex **6** with water (**6** + H_2O → **3** + HCOOH, $\Delta E^{\ddagger}$ = 143 kJ/mol; Scheme 5).

It is also interesting to compare the expected overall catalytic performance (turnover frequency, TOF) of $Ru(CO)_5$ in the WGSR with that of $Fe(CO)_5$. In many cases this is possible using the energetic span model recently proposed by Kozuch and Shaik,[30] where the so-called energetic span δE between a TOF-determining intermediate (TDI) and a TOF-determining transition state (TDTS) can be regarded as an effective barrier for the overall catalytic reaction (see ref 30 for further details and precise definitions). A preliminary, qualitative analysis of our system using a simplified version of the energetic span model suggests that both catalysts show similar performance within the estimated error bars of our calculations (energetic span δE = 147 kJ/mol for $Ru(CO)_5$ and δE = 139 kJ/mol for $Fe(CO)_5$ assuming $TSH_{6\rightarrow 3}$ as the TDTS and **6** as the TDI; δE = 130 kJ/mol for $Ru(CO)_5$ and δE = 118 kJ/mol for $Fe(CO)_5$ assuming $\mathbf{3}_H$ as the TDI; the two-state approximation has been employed; see the Supporting Information for more details). Given the reported experimental data mentioned in the Introduction which suggest that the catalytic efficiency of ruthenium carbonyls in WGSR is higher than that of $Fe(CO)_5$,[1c] it appears that our present data and analysis do not reproduce this experimental trend. This, in turn, would imply that yet other pathways, possibly involving polynuclear carbonyl clusters which have not been considered here, might be accessible for the ruthenium catalyst with lower effective barriers.

However, as has been discussed before,[5a] the prevalence of the various mechanistic proposals and catalytic turnover frequency will also depend on the reaction conditions such as total pressure: i.e., association steps will be favored by high pressure, while dissociative steps will profit thermodynamically from low-pressure conditions. Likewise, the partial pressures (i.e., concentrations) of CO, H_2O, CO_2, and H_2 will affect the kinetics of the individual steps and hence determine the catalytic productivity of each of the alternative catalytic cycles. A detailed discussion of all possible reaction conditions is beyond the scope of the present study. All pathways have to be considered in such kinetic simulations. One attractive feature of the classical mechanism A (Scheme 2) is the absence of any high-barrier steps, the rates of which are expected to show significant total pressure dependence. On the other hand, in the formic acid mechanism D, the catalytic cycle can proceed either from hydride species **3** via hydrometalation of CO_2 to yield **2** (activation barrier of $\Delta E^{\ddagger}$ = 91 kJ/mol) or via hydrometalation of CO to yield **6** (activation barrier of $\Delta E^{\ddagger}$ = 146 kJ/mol). In reaction setups designed to produce hydrogen via the WGSR, the reaction will be processed in a way so as to maintain high CO pressures and low CO_2 pressures. Such conditions tend to favor hydrometalation of CO (**3** + CO → **4**), despite its high activation barrier. Please note that a full kinetic analysis of the complex reaction network summarized in Figure 3 that takes into account various reaction conditions (as used in the abforementioned experiments) will be necessary to decide the relative performance of the ruthenium catalyst vs $Fe(CO)_5$ and other catalysts, which is beyond the scope of the present study.

5. CONCLUSIONS

In this report we have compared the reaction energies and activation barriers of several alternative mechanistic pathways in the ruthenium pentacarbonyl catalyzed water-gas shift reaction using density functional calculations including solution effects. For each path, the steps with the highest barriers have been identified. Our analysis shows, within the accuracy of the density functional methods used, that in addition to the classical mechanism, which involves a protolysis reaction, also an alternative pathway including the formation of formic acid may be competitive and has to be taken into account. Other catalytic cycles appear to be less favorable but might become relevant depending on the reaction conditions: i.e., the partial pressures of the reactants involved.

Our results show the importance of solvent effects, even in an approximate manner, in order to make predictions about the likeliness of mechanisms of the base-induced WGSR. In the gas phase, the classical mechanism appears unrealistic due to a very endothermic protolysis step. This step only becomes possible due to solvent effects. Our calculations furthermore predict that

dx.doi.org/10.1021/ic301539q | Inorg. Chem. 2013, 52, 4786−4794

water molecules can act as a proton relay in some (but not all) transition states, leading to a reduction of the computed activation barrier in these cases.

Given the tendency of ruthenium to form polynuclear carbonyl clusters, an interesting question is whether $Ru(CO)_5$ is really the active catalyst or if cluster compounds open other low-energy reaction paths. Recent successes in efficiently catalyzing the WGSR at very low temperatures (ultra-low-temperature WGSR) using ruthenium chloro carbonyl complexes in supported ionic liquid solution[8] show that an optimization of the ligand sphere might lead to still better catalysts. Further theoretical investigations will help to better understand and to optimize these complex catalyst systems.

■ ASSOCIATED CONTENT

Supporting Information

Text, tables, and a figure giving additional information on computational details, complementary B3LYP data, data on $Fe(CO)_5$ catalysis, the influence of the basis set, further details on solvation effects, a free energy diagram, and *XYZ* geometries of intermediates and transition states. This material is available free of charge via the Internet at http://pubs.acs.org.

■ AUTHOR INFORMATION

Corresponding Author

*E-Mail: wolfgang.hieringer@chemie.uni-erlangen.de.

Notes

The authors declare no competing financial interest.

■ ACKNOWLEDGMENTS

This work was conducted within the framework of the Cluster of Excellence "Engineering of Advanced Materials" granted to the University of Erlangen. We thank Sebastian Werner and Mehmet Ali Celik for helpful discussions and Sebastian Kozuch for advice and for providing us with his AUTOF software for performing the energetic span analysis.

■ REFERENCES

(1) (a) Ford, P. C. *Acc. Chem. Res.* **1981**, *14*, 31−37. (b) Laine, R. M. *J. Mol. Catal.* **1988**, *44*, 357−387. (c) Jacobs, G.; Davis, B. H. *Catalysis* **2007**, *20*, 122−285. (d) Newsome, D. S. *Catal. Rev. Sci. Eng.* **1980**, *21*, 275−318.

(2) (a) Ford, P. C.; Rinker, R. G.; Ungermann, C.; Laine, R. M.; Landis, V.; Moya, S. A. *J. Am. Chem. Soc.* **1978**, *100*, 4595−4597. (b) Sunderlin, L. S.; Squires, R. R. *J. Am. Chem. Soc.* **1993**, *115*, 331−343.

(3) Torrent, M.; Solà, M.; Frenking, G. *Organometallics* **1999**, *18*, 2801−2812.

(4) Barrows, S. E. *Inorg. Chem.* **2004**, *43*, 8236−8238.

(5) (a) Rozanska, X.; Vuilleumier, R. *Inorg. Chem.* **2008**, *47*, 8635−8640. (b) Zhang, F.; Zhao, L.; Xu, C.; Chen, Y. *Inorg. Chem.* **2010**, *49*, 3278−3281.

(6) Chen, Y.; Zhang, F.; Chunming, X.; Gao, J.; Zhai, D.; Zhao, Z. *J. Phys. Chem. A* **2012**, *116*, 2529−2535.

(7) Kuriakose, N.; Kadam, S.; Vanka, K. *Inorg. Chem.* **2012**, *51*, 377−385.

(8) (a) Werner, S.; Szesni, N.; Fischer, R. W.; Haumann, M.; Wasserscheid, P. *Phys. Chem. Chem. Phys.* **2009**, *11*, 10817−10819. (b) Werner, S.; Szesni, N.; Bittermann, A.; Schneider, M. J.; Härter, P.; Haumann, M.; Wasserscheid, P. *Appl. Catal., A* **2010**, *377*, 70−75.

(9) Elschenbroich, C. *Organometallics*, 3rd ed.; Wiley-VCH: New York, 2006.

(10) Hastings, W. R.; Roussel, M. R.; Baird, M. C. *J. Chem. Soc., Dalton Trans.* **1990**, 203−205.

(11) Laine, R. M.; Rinker, R. G.; Ford, P. C. *J. Am. Chem. Soc.* **1977**, *99*, 252−253.

(12) (a) Ahlrichs, R.; Bär, M.; Häser, M.; Horn, H.; Kölmel, C. *Chem. Phys. Lett.* **1989**, *162*, 165. (b) Ahlrichs, R.; Furche, F.; Hättig, C.; Klopper, W. M.; Sierka, M.; Weigend, F. et al. *TURBOMOLE 6.2 program package*; University of Karlsruhe, Karlsruhe, Germany; www.turbomole.com.

(13) Becke, A. D. *Phys. Rev. A* **1988**, *38*, 3098.

(14) Perdew, J. P. *Phys. Rev. B* **1986**, *33*, 8822.

(15) (a) Becke, A. D. *J. Chem. Phys.* **1993**, *98*, 5648. (b) Stephens, P. J.; Devlin, F. J.; Chabalowski, C. F.; Frisch, M. J. *J. Phys. Chem.* **1994**, *98*, 11623−11627.

(16) Weigend, F.; Ahlrichs, R. *Phys. Chem. Chem. Phys.* **2005**, *7*, 3297−3305.

(17) Kendall, R. A.; Dunning, T. H.; Harrison, R. J. *J. Chem. Phys.* **1992**, *96*, 6796.

(18) (a) Schäfer, A.; Klamt, A.; Sattel, D.; Lohrenz, J. C. W.; Eckert, F. *Phys. Chem. Chem. Phys.* **2000**, *2*, 2187−2193. (b) Klamt, A.; Schüürmann, G. *J. Chem. Soc., Perkin Trans. 2* **1993**, 799−805.

(19) Weingärtner, H. *Angew. Chem., Int. Ed.* **2008**, *47*, 654−670.

(20) (a) Ruelle, P.; Kesselring, U. W.; Nam-Tran, H. *J. Am. Chem. Soc.* **1986**, *108*, 371−375. (b) Ruelle, P. *J. Am. Chem. Soc.* **1987**, *109*, 1722−1725.

(21) Lane, K. R.; Lee, R. E.; Sallans, L.; Squires, R. R. *J. Am. Chem. Soc.* **1984**, *106*, 5767−5772.

(22) Pearson, R. G.; Mauermann, H. *J. Am. Chem. Soc.* **1982**, *104*, 500−504.

(23) The "*pV* + *TS*" penalty for bimolecular reactions amounts to 30−40 kJ/mol (see section 2), which would more than counteract all energy benefits. We were able to optimize precursor complexes with weakly coordinated water molecules (binding energies up to 3 kJ/mol; see above), on the basis of which the reactions with additional water molecule in the transition states can be considered unimolecular rather than bimolecular. The prevalence and properties of such complexes in real solution is unclear, however. In the remaining part, we will not explicitly refer to such weakly bound aqua complexes for simplicity.

(24) Grice, N.; Kao, S. C.; Pettit, R. *J. Am. Chem. Soc.* **1979**, *101*, 1627−1628.

(25) Our linear transit calculations have been performed as a series of constrained geometry optimizations. In each step of the series the Ru···O distance, which is part of the RuH···(OH) fragment in **3**, has been fixed while all other degrees of freedom have been optimized. This distance has been decreased stepwise from a large distance until a transfer of the hydride (bound to Ru) to the incoming hydroxide occurred. The energy of the highest point obtained on the relaxed energy−distance curve provides our (upper) estimate for the transition state energy.

(26) Amovilli, C.; Floris, F. M.; Solà, M.; Tomasi, J. *Organometallics* **2001**, *20*, 1310−1316.

(27) The linear transit calculation has been performed as a series of constrained geometry optimizations. In each step of the series, both Ru···H distances have been fixed to some number while all other degrees of freedom have been optimized. The Ru···H distances have been decreased stepwise from a large distance (where the two hydrogen atoms form a H_2 molecule) until H_2 dissociation occurs to form a ruthenium dihydride species (nonbonding H···H distance) at a small Ru···H distance. The resulting energy vs distance curve showed no maximum, indicating the absence of a pronounced transition structure.

(28) Niu, S. Q.; Hall, M. B. *Chem. Rev.* **2000**, *100*, 353−405.

(29) (a) Guitou-Guichemerre, M.; Chambaud, G. *J. Chem. Phys.* **2005**, *122*, 204325. (b) Morris, R. H. *Coord. Chem. Rev.* **2008**, *252*, 2381−2394.

(30) (a) Kozuch, S. *WIREs Comput. Mol. Sci.* **2012**, *2*, 795−815. (b) Kozuch, S.; Shaik, S. *Acc. Chem. Res.* **2011**, *44*, 101−110. (c) Uhe, A.; Kozuch, S.; Shaik, S. *J. Comput. Chem.* **2011**, *32*, 978−985.